Journal of Computer Science and Artificial Intelligence
ISSN: 3078-8242 (Print), ISSN: 3078-2309 (Online) | Vol. 7, No. 2, 2026

IIR Digital Filter Implementation via Red-billed Blue Magpie Optimization Algorithm

Layan Deng

Design and Engineering, Hunan Normal University, Changsha, 410081, China

Abstract: To overcome the insufficient stop-band attenuation and poor stability of conventional IIR filter design, this paper introduces the Red-billed Blue Magpie Optimization (RBMO) algorithm for the synthesis of 8th-order infinite-impulse-response digital filters. By emulating the collective intelligence of red-billed blue magpies, RBMO integrates a tri-modal "hop-walk-fly" search strategy with an "information-sharing & food-storing" cooperation mechanism, achieving an effective balance between global exploration and local exploitation. A pole-radius constraint is embedded to guarantee BIBO stability, while a unified fitness function that simultaneously penalizes pass-band magnitude error, peak stop-band ripple, and weighted transition-band deviation converts the design task into a single-objective optimization problem. Extensive simulations on low-pass, high-pass, band-pass and band-stop specifications demonstrate that the proposed scheme significantly reduces pass-band peak ripple, stop-band amplitude and transition-band error. The optimized coefficients, visualized through magnitude–frequency curves and pole-zero maps, corroborate the feasibility and practical potential of RBMO in high-performance IIR filter design.

Keywords: Digital Filter, Filter Design, Infinite Impulse Response (IIR) Filter, Red-billed Blue Magpie Optimization (RBMO), Global Optimization.

1. Introduction

Infinite Impulse Response (IIR) digital filters are typically capable of achieving sharp transition bands with a relatively low filter order, thereby significantly reducing computational complexity [1]. When realizing the same stopband attenuation, IIR structures require 40% to 60% fewer multipliers compared to Finite Impulse Response (FIR) filters, a characteristic particularly valuable for resource-constrained embedded systems [2]. However, while the bilinear transform method for IIR filter design is straightforward to implement, it often introduces frequency warping during the conversion between the analog and digital domains. This is accompanied by inherent nonlinear phase characteristics, making it difficult for filters designed through such conventional methods to meet the stringent requirements of high-precision applications [3, 4].

To overcome the limitations of traditional approaches, researchers have increasingly turned to intelligent optimization algorithms. In 1992, Benvenuto et al [5]. Attempted to apply the simulated annealing algorithm to filter design, but encountered issues with low efficiency. Subsequently, swarm intelligence algorithms became a focal point in this research area. In 2014, Saha et al [6]. Introduced the gravitational search algorithm for optimizing IIR filters, enhancing population diversity through a gravitational model and incorporating a wavelet mutation strategy to effectively mitigate the premature convergence issue common in particle swarm optimization. Mukherjee et al [7]. Introduced the Whale Optimization Algorithm (WOA) in 2017 for designing low-order FIR filters, evaluating filter efficiency by calculating passband ripple and stopband attenuation; the convergence curves of the designed FIR filters demonstrated stable convergence trends throughout the search space. The improved firefly algorithm (IFA) proposed by Dash et al [8]. I n 2020 provided a stable frequency magnitude response and exhibited strong performance in designing specific stopband IIR filters. In 2022, Jiang Jingyu et al [9]. Leveraged the Harris Hawks Optimization (HHO) algorithm's advantages in strong global search capability and few parameters to solve IIR digital filter design problems, opening a new avenue in this field. Dewangan et al [10]. Proposed using the Sparrow Search Algorithm (SSA) in 2024 to design 8th-order IIR filters, demonstrating enhanced accuracy and efficiency in optimizing key parameters such as peak stopband attenuation and transition band width.

Despite these advancements, existing methods still face unavoidable shortcomings: a single algorithm often struggles to balance convergence speed and solution accuracy [11]; in multi-objective optimization contexts, the trade-offs between different performance metrics have yet to be effectively reconciled [12]; furthermore, the design of high-order filters remains constrained by computational complexity. There is a persistent need to construct novel optimization frameworks to achieve further breakthroughs in both the efficiency and quality of filter design [13]. Based on this understanding, this paper introduces an IIR filter design method based on the Red-billed Blue Magpie Optimizer (RBMO). This algorithm, proposed by Fu et al 14]. In 2024, aims to establish a more rational balance between global exploration and local exploitation by simulating the foraging behavior and social cooperation mechanisms of red-billed blue magpies, thereby better addressing the multimodal and multi-objective optimization challenges inherent in IIR filter design. Concurrently, during the design process, filter stability is ensured by incorporating a pole radius constraint [15]. A fitness function is constructed that integrates the deviation of the passband magnitude response from the ideal value, the peak error of the stopband magnitude, and weighted control of the transition band, thus transforming the filter design problem into a single-objective optimization task.

2. Principle of the RBMO Algorithm

The Red-billed Blue Magpie Optimizer (RBMO) is a novel swarm intelligence optimization method, inspired by the collective foraging strategies and social cooperation

mechanisms exhibited by red-billed blue magpies in their natural environment. Due to its powerful exploratory mechanisms, such as "dynamic leadership rotation" and "storage-and-re-search," the RBMO algorithm has been widely applied to solve various critical engineering problems. At the initialization stage of the algorithm, N individuals are randomly generated to form the initial population,

$$x_{i,j} = lb_j + (ub_j - lb_j) \cdot rand(0,1) \quad (1)$$

Where i=1, 2, …, N, j=1, 2, …, D, and rand $(0, 1)$ denotes a uniformly distributed random number in the interval $[0, 1]$.

(1) Food Searching

During foraging, red-billed blue magpies adaptively switch their group size based on the context, ranging from small groups of 2–5 individuals to larger groups of 10 or more, thereby searching for resources in different organizational formations. They employ a combination of ground-based hopping and walking alongside canopy inspections, flexibly adjusting their strategies according to the environment and food abundance to ensure stable feeding. The position update formulas for small groups and large groups can be represented as follows, respectively:

$$X_i(t+1) = X_i(t) + \frac{1}{p}\sum_{m=1}^{p}\left(X_m(t) - X_{rs}(t)\right) \cdot Rand_2 \quad (2)$$

$$X_i(t+1) = X_i(t) + \frac{1}{q}\sum_{m=1}^{q}\left(X_m(t) - X_{rs}(t)\right) \cdot Rand_3 \quad (3)$$

Here, p, q represent the number of individuals within the group, $X_{rs}(t)$ is a randomly selected reference individual, and $Rand_2, Rand_3$ are random numbers uniformly distributed in [0, 1], serving as random perturbation terms. Equation (2) facilitates information exchange among populations by introducing random differential vectors, thereby enhancing global exploration capability. Equation (3), representing large-group foraging, enables the algorithm to explore unknown regions over a wider range, thus helping to avoid premature convergence.

(2) Prey Capture and Attack

When an individual locates a food position X_{food},the red-billed blue magpies switch to "siege mode." Small groups target small prey, employing tactics such as rapid pecking and aerial capture for efficient cooperation. Large groups, on the other hand, target larger prey for hunting. Their position update formulas are respectively expressed as:

$$X_i(t+1) = X_{food}(t) + CF \cdot \frac{1}{p}\sum_{m=1}^{p}\left(X_m(t) - X_i(t)\right) \cdot Rand_{n1} \quad (4)$$

$$X_i(t+1) = X_{food}(t) + CF \cdot \frac{1}{q}\sum_{m=1}^{q}\left(X_m(t) - X_i(t)\right) \cdot Rand_{n2} \quad (5)$$

Here, $CF = \left(1 - \left(\frac{t}{T}\right)\right)^{\left(2\times\frac{t}{T}\right)}$ is a control factor used to balance the exploration and exploitation capabilities of the algorithm. Its value decreases monotonically with the iteration count t, enabling the algorithm to maintain strong global search capability in the early stages while enhancing local convergence in the later stages. $Rand_{n1}, Rand_{n2}$ are random numbers following a standard normal distribution, introducing random perturbations during the attack phase.

(3) Food Storage

Red-billed blue magpies not only forage and hunt but also store surplus food in concealed places such as tree hollows. This mechanism ensures that the algorithm does not lose historically optimal solutions during the evolutionary process, helping the RBMO search agents explore the solution space more effectively to find the global optimum. Its mathematical model is as follows:

$$X_i(t+1) = \begin{cases} X_i(t), & \text{if } f(X_i(t+1)) > f(X_i(t)) \\ X_i(t+1), & \text{else} \end{cases} \quad (6)$$

Here, $f(X_i(t+1))$ and $f(X_i(t))$ represent the fitness values of the red-billed blue magpie's position before and after updating, respectively.

3. Optimal Design of IIR Digital Filters Based on the RBMO Algorithm

The system function of an IIR filter is given as follows, where the vectors $\{b_m\}$ and $\{a_m\}$ represent the filter coefficients:

$$H(z) = \frac{B(z)}{A(z)} = \frac{b_0 + b_1 z^{-1} + b_2 z^{-2} + \ldots + b_M z^{-M}}{1 + \alpha_1 z^{-1} + \alpha_2 z^{-2} \ldots + a_N z^{-N}} \quad (7)$$

Due to the lack of constraints on the pole radius in existing functions, there is no guarantee of the filter's stability margin. During quantization, poles located near the unit circle can lead to frequency response distortion and even the risk of filter instability. Therefore, the design criteria for high-order IIR filters require not only ensuring that the poles lie within the unit circle but also further restricting their radius to increase the stability margin and enhance accuracy. To this end, the pole-radius-constrained filter design method proposed by Lai Chunlu et al [15] is introduced. By combining the IIR filter transfer function with a cascade structure, the numerator of the transfer function is expressed as a single polynomial, and the denominator is expressed as cascaded second-order factors, specifically represented as follows:

$$H(z, b, a) = \frac{B(z)}{A(z)} = \frac{\sum_{r=0}^{N-1} b_r z^{-r}}{\prod_{k=1}^{\frac{N}{2}}(1 + \alpha_{k1} z^{-1} + \alpha_{k2} z^{-2})} \quad (8)$$

Here, $b = [b_0, b_1, \cdots, b_M]^T$ and $a = [a_{11}, a_{12}, \cdots, a_{N/2,1}, a_{N/2,2}]^T$ are the coefficient vectors of the denominator and numerator, respectively. Assume that the two poles of the k-th second-order section are in complex conjugate form:

$$z_{k1,2} = \rho_k e^{\pm j\theta_k} \quad (9)$$

Here, ρ_k is the pole radius, and θ_k is the pole angle. From the relationship between the roots and coefficients of a quadratic, we obtain: $a_{k1} = -2\rho_k cos\theta_k$, $a_{k2} = \rho_k^2$. The filter is stable when $\rho_k < 1$. The poles of the filter are the zeros of these second-order denominator polynomials. To further control the stability margin, an upper limit $r < 1$ for the pole radius is introduced, requiring: $\rho_k < r$, $k = 1,2, \ldots, N/2$.

Consequently, this pole constraint can be mapped from the complex plane into the coefficient space. For any stable second-order factor satisfying $|z| < r$, the stability condition can be transformed into a stability constraint inside the unit circle through the scaling transformation $z = rw$. If the coefficients of each second-order factor satisfy the following set of linear inequalities, then all pole radii of the IIR filter are guaranteed to be less than r.

$$\begin{cases} a_{k2} < r^2, \\ a_{k1} < r + \frac{a_{k2}}{r}, k = 1,2,\cdots,\frac{N}{2} \\ a_{k1} > -r - \frac{a_{k2}}{r}, \end{cases} \quad (10)$$

Let $z = e^{j\omega}$, The final magnitude-frequency response is given as follows:

$$\left|H(e^{j\omega})\right| = \sqrt{\left(Re\left(H(e^{j\omega})\right)\right)^2 + \left(Im\left(H(e^{j\omega})\right)\right)^2} \quad (11)$$

Here, $Re(H(e^{jw}))$ is the real part of the magnitude-frequency response, $Im(H(e^{jw}))$ is the imaginary part.

The ideal magnitude-frequency response for a filter, such as a bandpass filter is defined as:

$$|H_{BP}(w)| = \begin{cases} 0, & 0 \le w < w_{s1} \\ 1, & w_{p1} < w \le w_{p2} \\ 0, & w_{s2} \le w \le \pi \end{cases} \quad (12)$$

Where, w_{s1}, w_{s2} represent the stopband boundaries, and w_{p1}, w_{p2}represent the passband boundaries.

Furthermore, due to the highly nonlinear and multimodal nature of the objective function in IIR filter design, traditional methods and some intelligent optimization algorithms are heavily dependent on the initial solution and search path during the process. Their global exploration capability is often insufficient, making them prone to premature convergence at local optima. While reducing step size or enhancing local search can improve solution accuracy, it often significantly decreases convergence speed, thus making it difficult to achieve an effective balance between convergence efficiency and solution accuracy. Therefore, a weighted least mean square error function is constructed as the objective function to find and minimize the error between the desired frequency response and the designed filter's frequency response. This aims to achieve higher stopband attenuation (SBA) and a steeper transition band, while simultaneously minimizing ripples in both the stopband and passband. The objective function is defined as follows:

$$f = \frac{1}{n_s}\sum_{i=1}^{N_s}|H_i(w) - w_s| + \frac{1}{n_p}\sum_{i=1}^{N_p}\left||H_i(w)| - 1 - w_p\right| + \eta\left(max(P_{tran})\right) \quad (13)$$

Where, w_s, w_p are the target magnitudes for the stopband and passband, respectively; n_s, n_p are the number of sampling points in the stopband and passband, respectively; P_{tran}epresents the linear deviation in amplitude within the transition band; and η is a smoothing penalty factor, set to 0.05 here, used to suppress fluctuations in the transition band and balance the weight of errors between the passband and stopband.

The RBMO optimization algorithm possesses adaptive adjustment capabilities during the iterative process, allowing it to maintain a relatively fast convergence speed while enhancing its potential to escape local optimum regions. Therefore, this paper selects this optimization algorithm to conduct structural design and performance comparison analysis focusing on the multi-objective nonlinear optimization problem of IIR filters, including stopband attenuation and transition band roll-off. The design optimization problem is formulated as:

$$\min\left(f(X)\right), X = [x_1, x_2, \cdots, x_D] \in R^D \quad (14)$$

Where $f(X)$ is the weighted least mean square error objective function, D is the dimension of the search space, X_{min} *and* X_{max} are the lower and upper bounds of the variables, respectively.

The specific steps for achieving the optimal design of digital filters based on the RBMO optimization algorithm are as follows:

Initialization. The initial population is randomly generated according to Equation (1). The fitness value is calculated based on Equation (13), and the global optimal individual position, X_{food}, is recorded.

Parameter Setting. The maximum number of iterations T, the total population size, and the dimensionality are set.

Iterative Search. For each iteration, the algorithm selects either the "foraging mode" or the "predation mode" based on a probability. If the foraging stage is selected, the individual position is updated using Equation (2) or Equation (3). If the predation stage is selected, the individual position is updated using Equation (4) or Equation (5). After the predation phase is completed, the storage mechanism described in Equation (6) is executed to filter and store the local optimal values. Finally, the global optimal individual, X_{food}, is updated.

Termination. When the maximum number of iterations is reached or the convergence condition is satisfied, the optimal solution X_{food} and its corresponding fitness value are obtained. The optimized coefficient matrix for the IIR digital filter is then output.

4. Experiments and Analysis

To verify the global optimization performance of the introduced Red-billed Blue Magpie Optimizer (RBMO), this paper selects four typical swarm intelligence optimization algorithms for comparison: the Gravitational Search Algorithm (GSA), the Harris Hawks Optimization (HHO) algorithm, the Sparrow Search Algorithm (SSA), and the Whale Optimization Algorithm (WOA). All algorithms were run under the same parameter settings and initial conditions. The variation of their fitness values during the iterative process is shown in Figure 1,

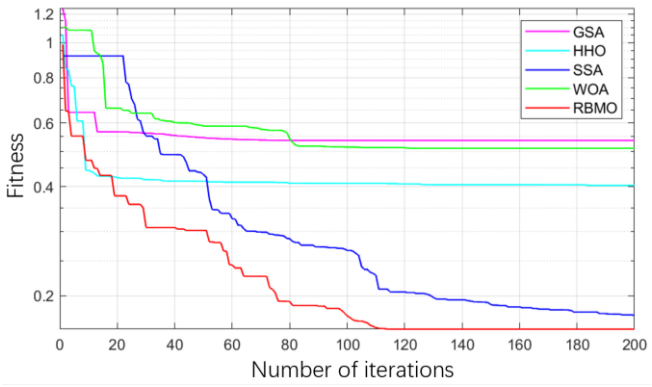

Figure 1. Fitness value variation curves of five optimization algorithms during the iterative process

As illustrated in the figure, all five algorithms exhibited a rapid downward trend in fitness value during the initial search phase. However, as the number of iterations increased, significant differences emerged in the convergence speed and final accuracy among the different algorithms. The RBMO algorithm demonstrated faster convergence speed and achieved a lower final fitness value throughout the optimization process. This indicates that the algorithm possesses a superior balance between the global exploration and local exploitation phases, enabling it to effectively escape

local optima traps and obtain a better global optimal solution.

Addressing the optimization problems for 8th-order low-pass, high-pass, band-pass, and band-stop IIR filters, extensive simulation comparisons were conducted on the optimization performance of the five algorithms: GSA, HHO, SSA, WOA, and RBMO. The design specifications for the four filter types are shown in Table 1, and the design indices adhered to by all algorithms are listed in Table 2.

Table 1. Filter Design Specifications

Filter Type	Passband Ripple (δ_p)	Stopband Ripple (δ_s)	Passband Normalized Cutoff Frequency (w_p)	Stopband Normalized Cutoff Frequency (w_S)
Low-Pass	0.01	0.001	0.45	0.5
High-Pass	0.01	0.001	0.35	0.3
Band-Pass	0.01	0.001	0.25, 0.65	0.3, 0.7
Band-Stop	0.01	0.001	0.25, 0.75	0.3, 0.7

Table 2. Control Parameters for GSA, HHO, SSA, WOA, and RBMO

Parameter / Algorithm Name	GSA	HHO	SSA	WOA	RBMO
Population Size	30	30	30	30	30
Number of Iterations	200	200	200	200	200
ε	0.0001	-	-	-	0.9
α	20	-	-	-	-
G_0	1000	-	-	-	-
rNORM	2	-	-	-	-
rPower	1	-	-	-	-

In this study, three aspects of the optimization algorithms were investigated: their accuracy, convergence speed, and stability. Tables 3 and 4 list the performance comparison of passband and stopband ripples, and the stopband attenuation performance for low-pass filters designed by different algorithms, respectively. Figure 2 resents a comparative gain plot in decibels (dB) for the 8th-order IIR low-pass filters designed by the different algorithms, and Figure 3 hows the comparative normalized gain plot for these 8th-order IIR low-pass filters. In these figures, the red curve represents the low-pass filter optimized by the RBMO algorithm introduced in this paper. The maximum stopband attenuations achieved are: 24.8407 dB, 50.6131 dB, 47.9107 dB, 60.8081 dB, and 72.0563 dB, respectively.

Table 3. Comparison of Passband and Stopband Ripple Performance for Low-Pass Filters Designed by Different Algorithms

Algorithm Name	Maximum Passband Ripple (Normalized)	Stopband Ripple (dB)		
		Maximum	Minimum	Average
WOA	0.160047	0.220070	0.000872	0.026632
GSA	0.138075	0.178081	0.007782	0.017723
HHO	0.104760	0.333804	0.002798	0.044621
SSA	0.069977	0.101265	0.000067	0.006968
RBMO	0.038921	0.066048	0.000237	0.003654

Table 4. Comparison of Stopband Attenuation Performance for Low-Pass Filters Optimally Designed by Different Algorithms

Algorithm Name / Parameter	Maximum Attenuation (dB)	Minimum Attenuation (dB)
GSA	24.8407	14.6235
SSA	47.9107	18.4632
HHO	50.6131	10.3191
WOA	60.8081	12.7696
RBMO	72.0563	25.2008

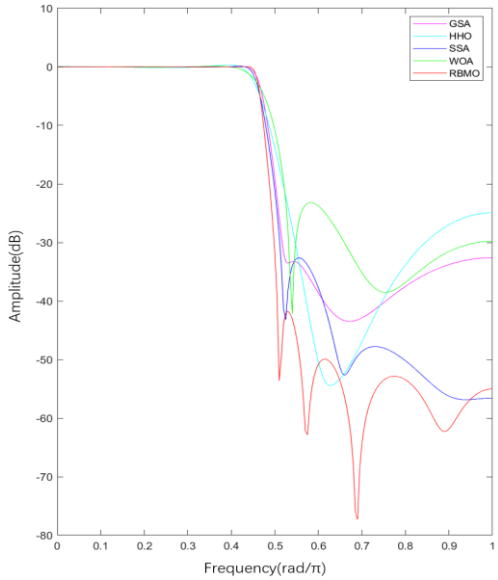

Figure 2. Magnitude-frequency response curves of low-pass filters

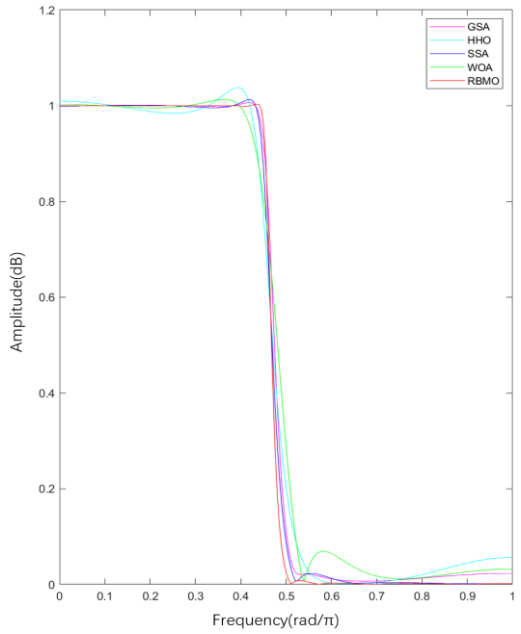

Figure 3. Normalized gain curves of low-pass filters

Table 5 lists the obtained optimal numerator coefficients (bk) and denominator coefficients (ak). It can be observed from Figure 4(e) that all poles of the IIR low-pass filter designed using the RBMO optimization algorithm lie within the unit circle. This satisfies the bounded-input, bounded-output (BIBO) stability condition, demonstrating its optimal stability performance among the compared algorithms.

Table 5. Comparison of Coefficients for Low-Pass Filters Optimally Designed by Different Algorithms

Algorithm	Numerator Coefficients (b_k)	Denominator Coefficients (a_k)
GSA	1.00000000 0.90154086 0.41278026 1.00000000 0.66681551 0.40158455 1.00000000 0.29280660 0.49824331 1.00000000 0.33005841 0.81437046	1.00000000 −0.02578942 0.07367292 1.00000000 −0.26416426 0.14105775 1.00000000 −0.20631035 0.61460596 1.00000000 −0.19832924 0.72019172
HHO	1.00000000 1.62503059 1.07389432 1.00000000 0.36273913 0.20314267 1.00000000 −0.47870621 0.30281877 1.00000000 0.36271370 0.69694673	1.00000000 0.00607378 0.00521487 1.00000000 −0.09195430 0.10829456 1.00000000 −0.49065758 0.40738798 1.00000000 −0.19687281 0.70459940
SSA	1.00000000 1.82993394 1.00564846 1.00000000 0.84342285 0.95023176 1.00000000 0.38420494 0.37953111 1.00000000 0.20877067 1.00141443	1.00000000 −0.13698792 0.10358045 1.00000000 0.06565220 0.15921756 1.00000000 −0.14096116 0.44645889 1.00000000 −0.25249653 0.83083838
WOA	1.00000000 1.18276319 1.32320704 1.00000000 0.92932327 0.79511398 1.00000000 0.71975227 0.85570844 1.00000000 0.41408507 0.38610626	1.00000000 0.00000000 0.00000000 1.00000000 0.33702382 0.27561672 1.00000000 0.14931514 0.36006369 1.00000000 −0.30795614 0.72244216
RBMO	1.00000000 1.55620606 0.72297668 1.00000000 0.63227152 0.09994316 1.00000000 0.64459518 0.90674455 1.00000000 0.18621365 1.00071401	1.00000000 −0.26717787 0.02251327 1.00000000 −0.37996364 0.22191194 1.00000000 −0.30422820 0.55995188 1.00000000 −0.24493939 0.87026544

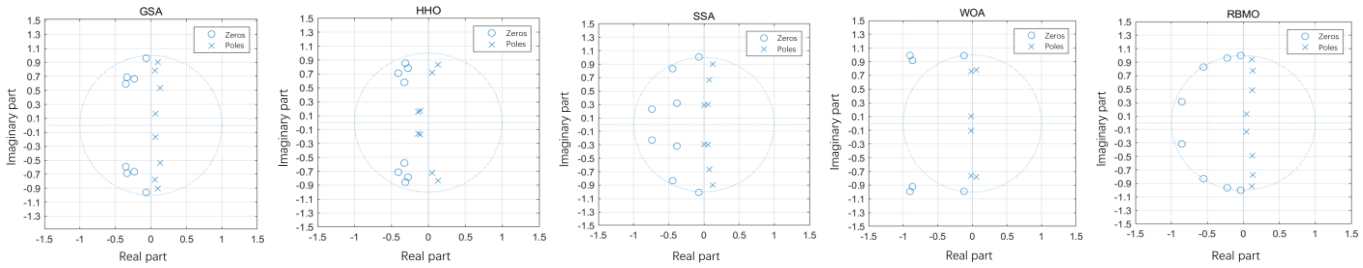

(a) GSA (b) HHO (c) SSA (d) WOA (e) RBMO

Figure 4. Pole-zero distribution plots of low-pass filters designed by five algorithms: GSA, HHO, SSA, WOA and RBMO

In summary, compared to the results obtained by other methods, the introduced RBMO optimization algorithm performs best in terms of stopband attenuation and exhibits the most optimal performance in stopband ripple for the 8th-order IIR low-pass filter.

Tables 6 and 7 list the performance comparison of passband and stopband ripples, and the stopband attenuation performance for high-pass filters designed by different algorithms, respectively. Figure 5 presents a comparative gain plot in decibels (dB) for the 8th-order IIR high-pass filters designed by the different algorithms, and Figure 6 shows the comparative normalized gain plot for these 8th-order IIR high-pass filters. In these figures, the red curve represents the high-pass filter optimized by the RBMO algorithm introduced in this paper. The maximum stopband attenuations achieved are: 40.1920 dB, 77.2145 dB, 77.7620 dB, 41.4815 dB, and 84.9376 dB, respectively.

Table 6. Comparison of Passband and Stopband Ripple Performance for High-Pass Filters Designed by Different Algorithms

Algorithm Name	Maximum Passband Ripple (Normalized)	Stopband Ripple (dB)		
		Maximum	Minimum	Average
HHO	0.396641	0.123580	0.001221	0.017944
WOA	0.395950	0.201203	0.006835	0.044068
GSA	0.290496	0.164546	0.007961	0.034383
SSA	0.066296	0.125095	0.001948	0.015692
RBMO	0.019317	0.038588	0.000220	0.003225

Table 7. Comparison of Stopband Attenuation Performance for High-Pass Filters Optimally Designed by Different Algorithms

Algorithm Name / Parameter	Maximum Attenuation (dB)	Minimum Attenuation (dB)
GSA	40.1920	15.9334
WOA	41.4815	13.5913
HHO	77.2145	22.1359
SSA	77.7620	16.5355
RBMO	84.9376	26.1256

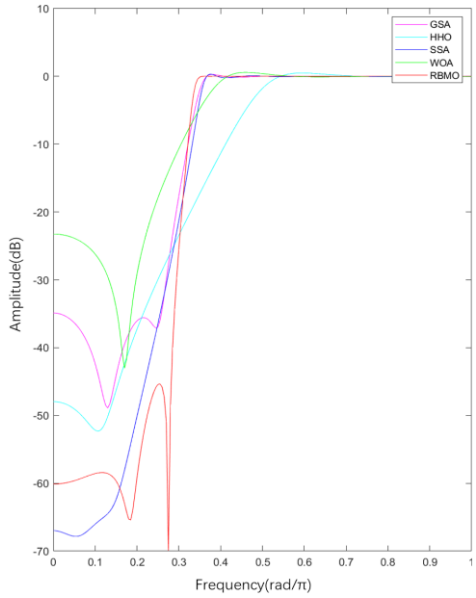

Figure 5. Magnitude-frequency response curves of high-pass filters

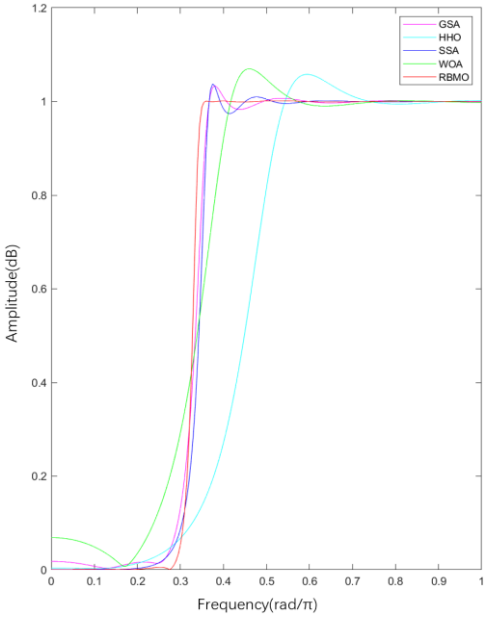

Figure 6. Normalized gain curves of high-pass filters

Table 8 lists the obtained optimal numerator coefficients (bk) and denominator coefficients (ak). Figure 9 shows the pole-zero plots of the 8th-order IIR high-pass filters designed using five different optimization algorithms, respectively. It can be observed that all poles of the IIR high-pass filter designed by the RBMO optimization algorithm in Figure 7(e) are located inside the unit circle, which ensures the bounded-input bounded-output (BIBO) stability condition, demonstrating the optimal stability performance.

Table 8. Comparison of Coefficients for High-Pass Filters Optimized by Different Algorithms

Algorithm	Numerator Coefficients (b_k)	Denominator Coefficients (a_k)
GSA	1.00000000 −0.98341500 0.25900203 1.00000000 −0.45548030 0.08590398 1.00000000 −0.46599577 0.09792113 1.00000000 −0.35599087 0.08427222	1.00000000 0.37207464 0.06620702 1.00000000 0.22109912 0.12659671 1.00000000 −0.08164772 0.42013417 1.00000000 −0.68274699 0.79377132
HHO	1.00000000 −0.00091278 −0.00013468 1.00000000 −1.29537323 0.43401690 1.00000000 0.02204207 0.08168299 1.00000000 −1.66064637 0.95365571	1.00000000 0.00002539 0.00007983 1.00000000 0.02825549 0.06023427 1.00000000 0.27864972 0.27116801 1.00000000 −0.62480708 0.76691968
SSA	1.00000000 −1.77596492 0.90360003 1.00000000 −0.29429587 0.03669219 1.00000000 −0.20626374 0.11880663 1.00000000 −1.36313110 0.98953319	1.00000000 −0.06479564 0.04554842 1.00000000 0.06488378 0.07495357 1.00000000 −0.36059862 0.40088071 1.00000000 −0.84699497 0.83226889
WOA	1.00000000 −0.18002805 −0.01657392 1.00000000 −1.98674682 1.16182538 1.00000000 −0.25970111 0.01888444 1.00000000 0.05812996 0.01038032	1.00000000 −0.07697786 0.00322533 1.00000000 0.07718030 0.00337735 1.00000000 0.38998991 0.14346708 1.00000000 −0.45044501 0.63987890
RBMO	1.00000000 −1.74674117 1.03366052 1.00000000 −1.54340385 0.65199888 1.00000000 −0.19593258 0.12621266 1.00000000 −1.28031454 0.98821281	1.00000000 0.26911061 0.07301324 1.00000000 −0.08544347 0.30980590 1.00000000 −0.59613229 0.63098267 1.00000000 −0.89649531 0.90032862

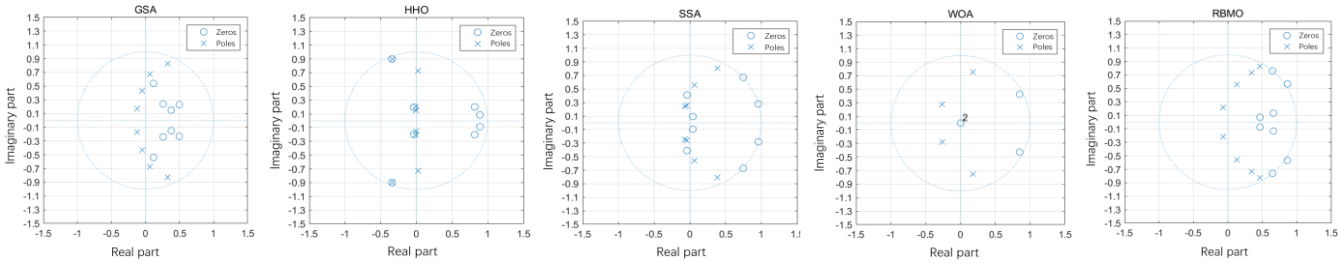

(a) GSA (b) HHO (c) SSA (d) WOA (e) RBMO

Figure 7. Pole-zero distribution plots of high-pass filters designed by five algorithms

In summary, compared to the results obtained by other methods, the introduced RBMO optimization algorithm performs best in terms of stopband attenuation and exhibits the most optimal performance in stopband ripple for the 8th-order IIR high-pass filter.

Tables 9 and 10 list the performance comparison of passband and stopband ripples, and the stopband attenuation performance for band-pass filters designed by different algorithms, respectively. Figure 8 presents a comparative gain plot in decibels (dB) for the 8th-order IIR band-pass filters designed by the different algorithms, and Figure 9 shows the comparative normalized gain plot for these 8th-order IIR band-pass filters. In these figures, the red curve represents the band-pass filter optimized by the RBMO algorithm introduced in this paper. The maximum stopband attenuations achieved are: 36.731452 dB, 34.479739 dB, 63.043584 dB, 33.155397 dB, and 101.615763 dB, respectively.

Table 9. Comparison of Passband and Stopband Ripple Performance for Band-Pass Filters Designed by Different Algorithms

Algorithm Name	Maximum Passband Ripple (Normalized)	Stopband Ripple (dB)		
		Maximum	Minimum	Average
WOA	0.471475	0.160142	0.018971	0.049239
HHO	0.386063	0.217549	0.016803	0.045952
GSA	0.089984	0.186173	0.013477	0.040931
SSA	0.071500	0.169139	0.000688	0.024888
RBMO	0.022949	0.120229	0.000008	0.012284

Table 10. Comparison of Stopband Attenuation Performance for Band-Pass Filters Optimally Designed by Different Algorithms

Algorithm Name / Parameter	Maximum Attenuation (dB)	Minimum Attenuation (dB)
WOA	33.155397	14.627090
HHO	34.479739	12.236176
GSA	36.731452	13.924746
SSA	63.043584	15.229163
RBMO	101.615763	18.298902

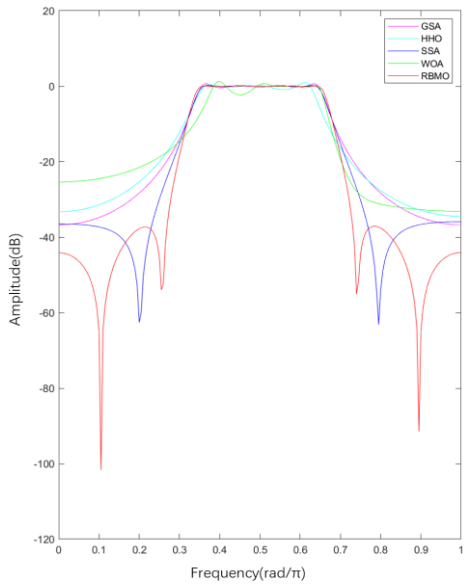

Figure 8. Magnitude-frequency response curves of band-pass filters

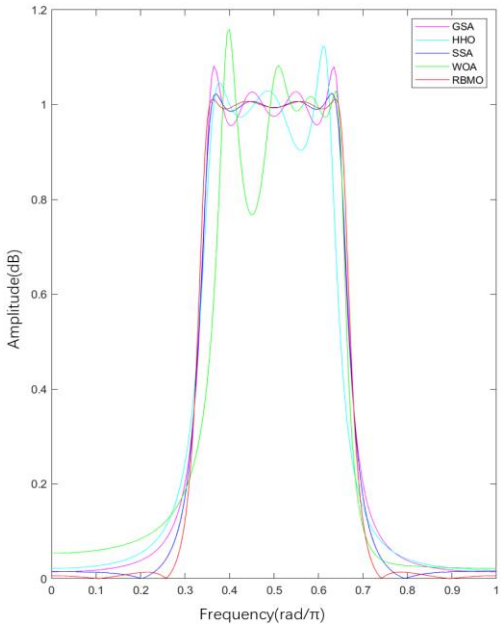

Figure 9. Normalized gain curves of band-pass filters

Table 11 Optimal Numerator Coefficients (b_k) and Denominator Coefficients (a_k) Obtained for Band-Pass Filters Designed by Different Algorithms. It can be observed from Figure 10(e) that all poles of the IIR band-pass filter designed using the RBMO optimization algorithm lie within the unit circle. This satisfies the bounded-input, bounded-output (BIBO) stability condition, demonstrating its optimal stability performance among the compared algorithms.

Table 11. Comparison of Coefficients for Band-Pass Filters Optimized by Different Algorithms

Algorithm	Numerator Coefficients (b_k)			Denominator Coefficients (a_k)		
GSA	1.00000000	−0.01406854	−0.05479396	1.00000000	0.28998328	0.69970676
	1.00000000	0.01314253	0.05386893	1.00000000	−0.28903983	0.69978179
	1.00000000	0.32841594	0.05216173	1.00000000	0.81144874	0.86253802
	1.00000000	−0.32749862	0.05649611	1.00000000	−0.81175184	0.86308921
HHO	1.00000000	−0.02626717	−0.03861912	1.00000000	−0.25701281	0.51179603
	1.00000000	0.23136186	0.03868414	1.00000000	0.02861430	0.62368027
	1.00000000	−0.23308696	0.05452809	1.00000000	−0.76586996	0.81373133
	1.00000000	−0.13307385	0.09598995	1.00000000	0.68243182	0.85679675
SSA	1.00000000	−0.00799620	−0.00363428	1.00000000	0.31910150	0.59675666
	1.00000000	−0.00459308	0.00384475	1.00000000	−0.31414925	0.59877773
	1.00000000	1.58839191	0.98847835	1.00000000	0.82873122	0.84032337
	1.00000000	−1.60754451	0.99693693	1.00000000	−0.82918965	0.84190742
WOA	1.00000000	0.00007998	−0.00006389	1.00000000	0.46297839	0.74408683
	1.00000000	0.13303305	0.11400577	1.00000000	0.02049749	0.80369837
	1.00000000	−0.02941038	1.72117163	1.00000000	−0.60675161	0.86733966
	1.00000000	1.56894870	1.42373899	1.00000000	0.85318604	0.89262754
RBMO	1.00000000	−1.89176493	0.99955658	1.00000000	−0.40279640	0.54986027
	1.00000000	1.89354131	1.00140663	1.00000000	0.40498693	0.55029731
	1.00000000	−1.38158834	1.00101118	1.00000000	−0.88328923	0.86235461
	1.00000000	1.37822655	1.00099345	1.00000000	0.88422986	0.86277726

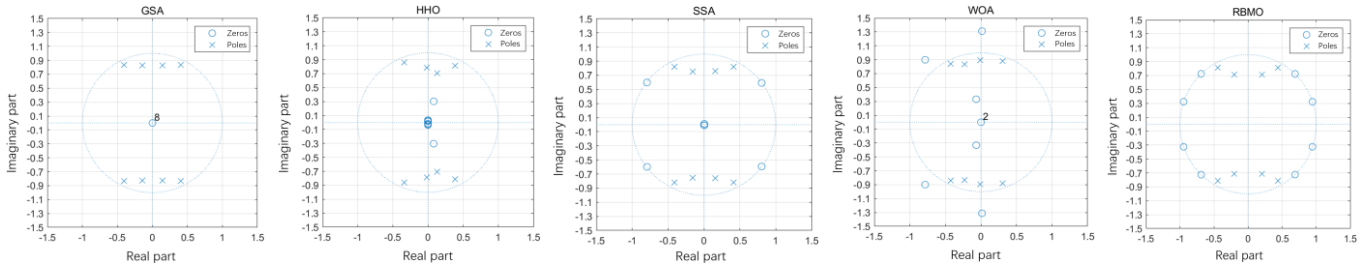

(a) GSA (b) HHO (c) SSA (d) WOA (e) RBMO

Figure 10. Pole-Zero Distribution Diagrams of Band-Pass Filters Designed by Five Algorithms: GSA, HHO, SSA, WOA, and RBMO

In summary, compared to the results obtained by other methods, the introduced RBMO optimization algorithm performs best in terms of stopband attenuation and exhibits the most optimal performance in stopband ripple for the 8th-order IIR band-pass filter.

Tables 12 and 13 list the performance comparison of passband and stopband ripples, and the stopband attenuation performance for band-stop filters designed by different algorithms, respectively. Figure 11 presents a comparative gain plot in decibels (dB) for the 8th-order IIR band-stop filters designed by the different algorithms, and Figure 12 shows the comparative normalized gain plot for these 8th-order IIR band-stop filters. In these figures, the red curve represents the band-stop filter optimized by the RBMO algorithm introduced in this paper. The maximum stopband attenuations achieved are: 71.964404 dB, 44.057305 dB, 51.397144 dB, 66.867914 dB, and 74.585249 dB, respectively.

Table 12. Comparison of Passband and Stopband Ripple Performance for Band-Stop Filters Designed by Different Algorithms

Algorithm Name	Maximum Passband Ripple (Normalized)	Stopband Ripple (dB)		
		Maximum	Minimum	Average
WOA	0.105588	0.808993	0.000441	0.253315
GSA	0.093525	0.828948	0.000251	0.177357
SSA	0.072295	0.865159	0.002652	0.128610
HHO	0.042104	0.919194	0.005931	0.255049
RBMO	0.031954	0.938071	0.000183	0.111564

Table 13. Comparison of Stopband Attenuation Performance for Band-Stop Filters Optimally Designed by Different Algorithms

Algorithm Name / Parameter	Maximum Attenuation (dB)	Minimum Attenuation (dB)
HHO	44.057305	0.252010
SSA	51.397144	1.126660
WOA	66.867914	1.601152
GSA	71.964404	1.577370
RBMO	74.585249	0.369948

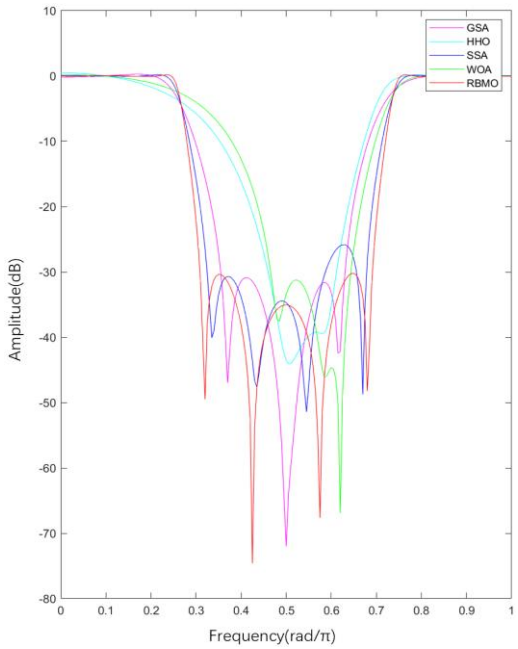

Figure 11. Magnitude-frequency response curves of band-stop filters

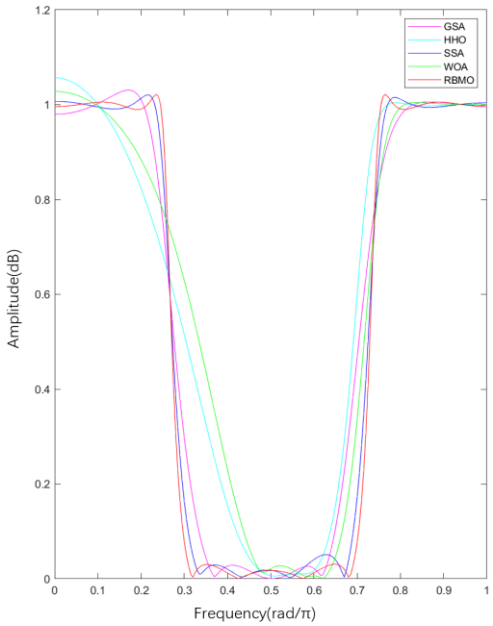

Figure 12. Normalized gain curves of band-stop filters

Table 14 Optimal Numerator Coefficients (b_k) and Denominator Coefficients (a_k) Obtained for Band-Stop Filters Designed by Different Algorithms. It can be observed from Figure 13(e) that all poles of the IIR band-stop filter designed using the RBMO optimization algorithm lie within the unit circle. This satisfies the bounded-input, bounded-output (BIBO) stability condition, demonstrating its optimal stability performance among the compared algorithms.

Table 14. Comparison of Coefficients for Band-Stop Filters Optimally Designed by Different Algorithms

Algorithm	Numerator Coefficients (b_k)	Denominator Coefficients (a_k)
GSA	1.00000000 −0.00703367 1.01169960 1.00000000 0.06237553 0.92577948 1.00000000 0.71555703 0.97922577 1.00000000 −0.78677272 0.98241603	1.00000000 −0.23737667 0.34024800 1.00000000 0.46714479 0.46339296 1.00000000 0.94298225 0.57274562 1.00000000 −1.12454339 0.63055870
HHO	1.00000000 0.00715684 1.12449798 1.00000000 0.17991519 0.72204781 1.00000000 0.06499693 0.65935946 1.00000000 0.53074362 0.90074052	1.00000000 −0.16240081 0.06621193 1.00000000 −0.34641830 0.35698673 1.00000000 0.18238414 0.60781961 1.00000000 1.03546320 0.69858242
SSA	1.00000000 −0.40517249 0.95637293 1.00000000 0.27898040 0.97431917 1.00000000 1.01345124 0.99258175 1.00000000 −0.97123993 0.97037899	1.00000000 −0.26286104 0.12935142 1.00000000 0.24098660 0.18229289 1.00000000 1.21115993 0.77845901 1.00000000 −1.23355040 0.78622362
WOA	1.00000000 −0.11864557 1.06244435 1.00000000 0.50561344 0.93308504 1.00000000 0.01744140 0.00364006 1.00000000 0.74024346 1.00266463	1.00000000 0.00000316 0.00001861 1.00000000 0.11760745 0.27755762 1.00000000 −0.34680447 0.28524268 1.00000000 1.10140088 0.67889140
RBMO	1.00000000 0.46112144 0.99879424 1.00000000 −0.46554712 1.00186724 1.00000000 1.08067677 1.00039235 1.00000000 −1.07914007 0.99964253	1.00000000 0.98286540 0.37795662 1.00000000 −0.98381446 0.37836157 1.00000000 1.27651623 0.85791649 1.00000000 −1.27669682 0.85792849

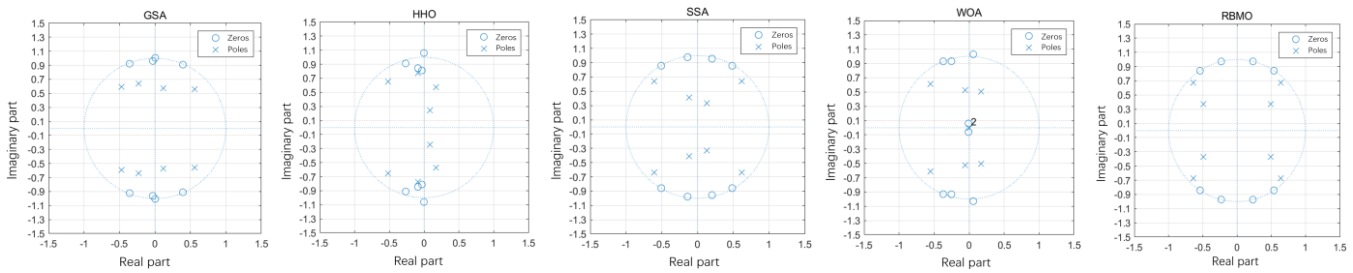

(a) GSA (b) HHO (c) SSA (d) WOA (e) RBMO

Figure 13. Pole-zero distribution plots of band-stop filters designed by five algorithms: (a) GSA, (b) HHO, (c) SSA, (d) WOA, and (e) RBMO

In summary, compared to the results obtained by other methods, the introduced RBMO optimization algorithm performs best in terms of stopband attenuation and exhibits the most optimal performance in stopband ripple for the 8th-order IIR band-stop filter.

5. Conclusion

This study has successfully designed a series of high-performance 8th-order IIR digital filters, including low-pass, high-pass, band-pass, and band-stop types. The design process introduced the novel Red-billed Blue Magpie Optimizer (RBMO) to approximate the ideal magnitude response. In the experimental investigation, the RBMO optimization algorithm achieved superior results compared to other algorithms across the four digital IIR filter design cases. The resulting filters all satisfied stability requirements and exhibited favorable stopband attenuation along with relatively smooth transition bands. Furthermore, the RBMO demonstrated fast convergence speed during the optimization process.

References

[1] Zhang, X. G., & Xu, Z. (2006). IIR digital filter optimization design and DSP implementation. Electronic Engineer, (3), 37–39. (in Chinese)

[2] Ji, S. Y., Li, L. T., Zhang, H. F., et al. (2016). Design and distortion correction of digital band-stop filter. Optical Instruments, 38(4), 346–349, 367. (in Chinese)

[3] Taylor, F. J. (2013). Digital filters: Principles and applications with MATLAB (J. H. Cheng & S. M. Yuan, Trans.). National Defense Industry Press. (in Chinese)

[4] Zheng, N. N., & Cheng, H. (2009). Digital signal processing. Tsinghua University Press. (in Chinese)

[5] Benvenuto, N., Marchesi, M., & Uncini, A. (1992). Applications of simulated annealing for the design of special digital filters. IEEE Transactions on Signal Processing, 40(2), 323. https://doi.org/10.1109/78.129483

[6] Saha, S. K., Kar, R., Mandal, D., et al. (2014). Gravitation search algorithm: Application to the optimal IIR filter design. Journal of King Saud University – Engineering Sciences, 26(1), 69–81. https://doi.org/10.1016/j.jksues.2013.02.001

[7] Mukherjee, A., Chakraborty, N., & Das, B. K. (2017). Whale optimization algorithm: An implementation to design low-pass FIR filter. In 2017 Innovations in Power and Advanced Computing Technologies (i-PACT) (pp. 1–5). https://doi.org/10.1109/IPACT.2017.8244928

[8] Dash, J., Dam, B., & Swain, R. (2020). Improved firefly algorithm based optimal design of special signal blocking IIR filters. Measurement, 149, 106986. https://doi.org/10.1016/j.measurement.2019.106986

[9] Jiang, J. Y., Zhang, H. M., & Liu, T. (2022). Design of IIR filter based on Harris Hawks optimization algorithm. Office Informatization, 27(23), 6–10. (in Chinese)

[10] Dewangan, S., Yadav, S., & Saha, S. K. (2024). IIR filter design using sparrow search algorithm. In 2024 15th International Conference on Computing Communication and Networking Technologies (ICCCNT) (pp. 1–6). https://doi.org/10.1109/ICCCNT61003.2024.10632418

[11] He, C. G. (2025). Research on grasshopper optimization algorithm and its application in digital filter [Master's thesis]. Anhui University of Science and Technology. (in Chinese)

[12] Agrawal, N., Kumar, A., Bajaj, V., et al. (2021). Design of digital IIR filter: A research survey. Applied Acoustics, 172, 107669. https://doi.org/10.1016/j.apacoust.2020.107669

[13] Chauhan, S., Singh, M., & Aggarwal, A. K. (2023). Designing of optimal digital IIR filter in the multi-objective framework using an evolutionary algorithm. Engineering Applications of Artificial Intelligence, 119, 105803. https://doi.org/10.1016/j.engappai.2023.105803

[14] Fu, S., Li, K., Huang, H., et al. (2024). Red-billed blue magpie optimizer: A novel metaheuristic algorithm for 2D/3D UAV path planning and engineering design problems. Artificial Intelligence Review, 57(6), 134. https://doi.org/10.1007/s10462-024-10758-1

[15] Lai, C. L., Yao, T., & Wang, L. (2022). A new algorithm for IIR digital filter design with pole radius constraint. Research and Exploration in Laboratory, 41(8), 39–44. (in Chinese)